International Journal of Mining Science and Technology 35 (2025) 1713–1729

Contents lists available at ScienceDirect

International Journal of Mining Science and Technology

journal homepage: www.elsevier.com/locate/ijmst

Experimental investigation of anisotropy ratio evolution in coal permeability: Implications for underground compressed air energy and CO_2 storage

Tiancheng Zhang [a], Luwei Ding [a,*], Jimmy Xuekai Li [a], Yiran Zhu [a], Victor Rudolph [b], Zhongwei Chen [a,*]

[a] School of Mechanical and Mining Engineering, The University of Queensland, St Lucia 4072, Australia
[b] School of Chemical Engineering, The University of Queensland, St Lucia 4072, Australia

ARTICLE INFO

Article history:
Received 11 July 2025
Received in revised form 28 August 2025
Accepted 16 September 2025
Available online 25 October 2025

Keywords:
Anisotropy
Permeability
Gas adsorption
Effective stress
Cleat compressibility
Compressed air energy storage

ABSTRACT

Reliable forecasting of coal seam gas production and gas injectivity (e.g., CO_2 or air) requires an accurate understanding of coal's anisotropic permeability, which governs the directional flow of gas. Although the anisotropic nature of coal permeability is well recognized, little attention has been paid to how this ratio evolves with changes in effective stress or with the injection of gases that have different affinities to coal. In this work, more than 600 permeability tests were conducted on eight cubic Australian coal samples using He, N_2 and CO_2 gases under varying effective stresses, providing a comprehensive dataset that allows the combined effects of effective stress and gas adsorption on permeability anisotropy to be robustly assessed on the same samples. The results demonstrated that all coal samples exhibited evident permeability anisotropy, with ratios ranging from 1.11 to 6.55. For the first time, quantitative relationships between the anisotropy ratio, effective stress, and initial permeability were established for each of the three injection gases, highlighting how gas adsorption and effective stress changes both anisotropic permeability magnitude and ratio. These findings provide new insights into the directional flow behavior of gases in coal seams, with implications for underground compressed air energy storage and CO_2 sequestration.

1. Introduction

Coal seams serve as reservoirs for coal seam gas (CSG), an important energy source, and as storage sites for CO_2 geological sequestration and underground compressed air energy storage (CAES) [1–5]. Coal is an anisotropic porous medium due to its unique cleat system, which is the primary fluid flow pathway in coal seams [6–8]. In most coal seams, the permeability is highest in the direction parallel to the bedding planes, often several times greater than that in the direction perpendicular to the bedding planes [9]. This anisotropy strongly influences permeability and dictates the optimal orientation of boreholes, including lateral wells [10]. Therefore, to maximize gas extraction and gas injection efficiency, borehole placement and orientation should be fully designed to align with the anisotropy permeability of coal.

Permeability changes in coal occur during the CSG extraction or gas injection, primarily due to two mechanisms [11–14]: mechanical deformation caused by pore pressure changes and coal matrix swelling or shrinkage induced by gas (e.g. CO_2 and CH_4) adsorption or desorption. To capture these effects, a series of experiments and simulations have been conducted to develop the permeability models [15]. Currently, many classical permeability models based on isotropic assumptions have been proposed, such as Palmer and Mansoori's model [16], Pan and Connell's model [17] and Shi and Durucan's model [18]. These models have demonstrated good performance in predicting permeability changes caused by variations in effective stress and gas adsorption/desorption impacts. However, later studies have found that cleat compressibility and adsorption-induced deformation also exhibit significant anisotropy, which may affect the evolution of permeability [19–21]. Therefore, despite these findings, how to integrate permeability changes induced by effective stress variations and matrix swelling/shrinkage with permeability anisotropy remains to be further investigated [22,23].

Previous experimental studies have investigated the anisotropic permeability of coal by measuring cylindrical samples cored along different directions relative to the cleat orientation [24–27]. However, due to the significant variability between individual coal samples, cubic samples have gained wider acceptance compared to cylindrical ones [28,29]. Some experimental studies showed that cubic coal samples also exhibited significant anisotropic permeability [30]. Moreover, both cleat orientation and stress conditions can affect the coal anisotropic permeability [28]. To quantify

* Corresponding authors.
E-mail addresses: luwei.ding@uq.edu.au (L. Ding), zhongwei.chen@uq.edu.au (Z. Chen).

https://doi.org/10.1016/j.ijmst.2025.09.006
2095-2686/

anisotropy, the anisotropy ratio and the degree of anisotropy have been proposed [31,32]. However, the quantification of anisotropy variation with effective stress and pore pressure remains little explored.

To address this gap, eight cubic coal samples from Bowen Basin, Australia are prepared in this work. More than 600 permeability measurements are performed to study the effects of effective stress and gas adsorption on coal anisotropy evolution. A new set of quantitative relationships between the anisotropy ratio, effective stress, and initial permeability are first established for helium gas, N_2 and CO_2, respectively, providing new insights into coal permeability anisotropy. The correlation of initial permeability and gas adsorption with coal cleat compressibility is also investigated.

2. Permeability testing on cubic coal samples: Setup and validation

2.1. Geological setting of coal seams

The samples were collected from Goonyella Middle (GM) seam of the Bowen Basin, which is a north-south trending basin, elongate sedimentary basin located in east-central Queensland and northern New South Wales, Australia. The GM seam is the thickest and most laterally extensive seam in the region, making it favorable for economic CSG exploration [33]. A cross-section of the Bowen Basin is shown in Fig. 1.

The GM seam is classified as high-volatile bituminous rank, with a mean maximum vitrinite reflectance ranging from 1.1% to 1.2%. It contains 13%–23% mineral matter, mainly quartz (15%–60%), kaolinite (20%–50%), and interstratified illite/smectite (15%–30%), with minor siderite (3%–6%) and trace amounts of ankerite [34].

2.2. Experiment apparatus

The permeability experimental system used in this work is shown in Fig. 2. The setup includes a 38 mm diameter core holder, three ISCO pumps, two double-ended cylinders of 75 mL, two pressure transducers, and a vacuum pump. It is designed to measure permeability using the transient method [35].

2.3. Experimental procedure

The coal blocks were collected from Goonyella Middle Seam in Bowen Basin, Australia. These coal blocks were then cut into

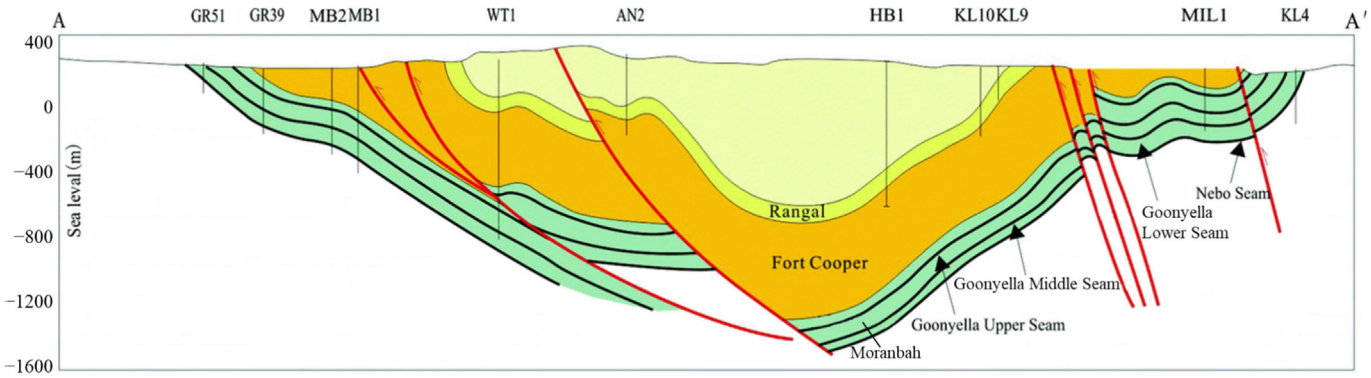

Fig. 1. General cross-section of the Bowen Basin [33].

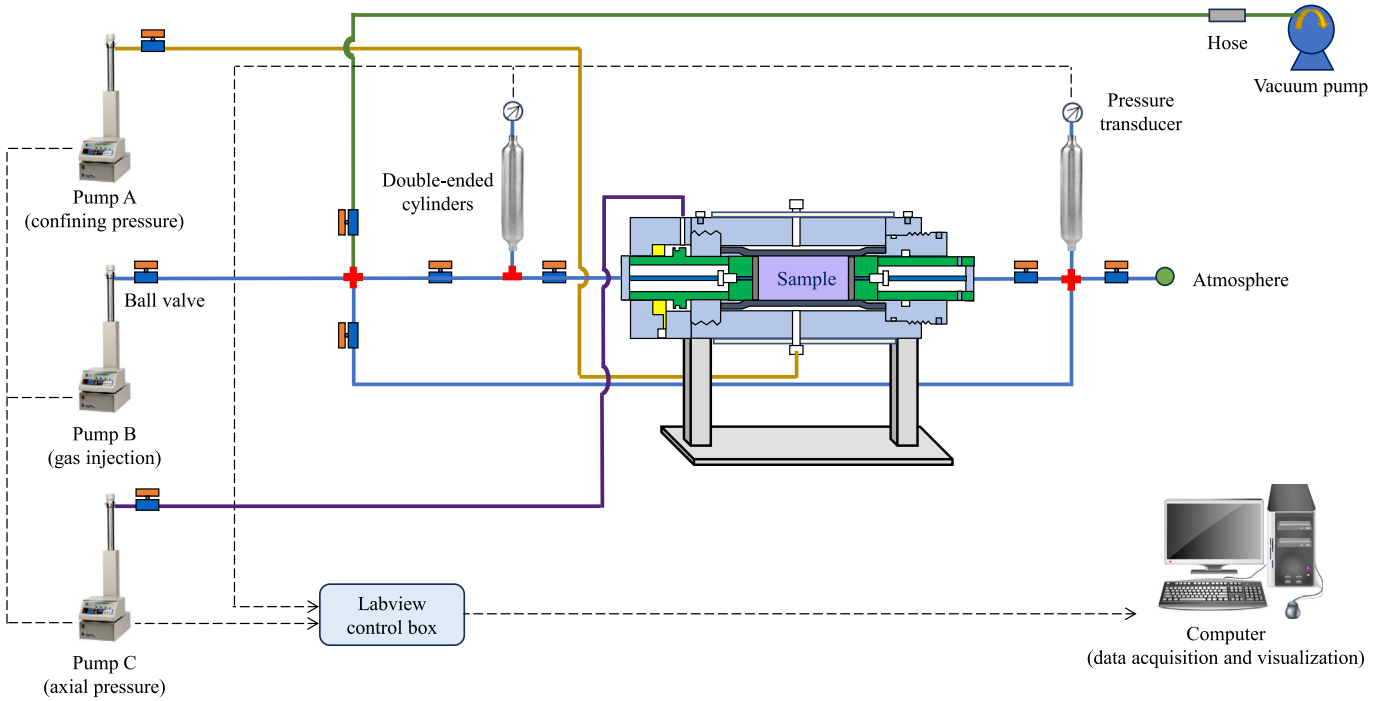

Fig. 2. Schematic diagram of permeability experimental system.

20 mm cubes along the cleat orientations, and each face was polished to ensure a flat surface. However, the exact horizontal and vertical directions could not be definitively identified, so the directions are simply labeled as A, B, and C. Then, the cubic sample was inserted into a 3D-printed rubber sleeve with a cubic-shaped cavity and a circular outer surface, allowing it to fit securely into the core holder, as shown in Fig. 3a. In addition, before conducting permeability tests, the coal samples were placed in the core holder and were subjected to cyclic confining pressure loading and unloading to minimize the impact of irreversible deformations on permeability measurements [36,37].

The initial permeability in all directions was measured using helium (He) gas under an axial pressure of 1.0 MPa, a confining stress of 1.5 MPa and a pore pressure of 0.5 MPa on the eight samples. The results of cubic coal samples are summarized in Table 1. In this table, k_A, k_B and k_C represent the initial permeability values measured along the A, B, and C directions, respectively. The parameter k_0 denotes the maximum permeability value among the three directions, indicating the degree of fracture development, and is used to represent the initial permeability of each cubic sample in the subsequent discussion.

After initial permeability tests, three different gases (i.e., He, N_2 and CO_2) were used in the following permeability tests. For the first direction (A direction), the permeability was first measured using helium at a constant pore pressure of 0.5 MPa, confining pressure of 1.5 MPa and an axial pressure of 1.0 MPa (with the effective stress defined as confining stress minus the pore pressure, yielding a value of 1.0 MPa). The confining pressure started from 1.5 MPa and increased by 1.0 MPa at each step until reaching 4.5 MPa. Then, the pore pressure increased to 1.0 MPa and confining pressure was set to 2.0 MPa. The confining pressure started from 2.0 MPa and increased by 1.0 MPa at each step until reaching 5.0 MPa. For all tests, the axial was maintained at 1.0 MPa. For N_2 and CO_2 injections, the pore pressure was maintained until adsorption reached equilibrium, after which permeability tests were conducted in the same manner as for helium. After the measurements for each gas, the coal sample was vacuumed for 24 h to remove the residual gas. To ensure the integrity of the coal samples, relatively low-pressure conditions were selected for both effective stress and pore pressure in this work [30,38].

Once the tests for the A direction were completed, the sample was removed from the core holder and repositioned to test the other two directions (B and C directions) with the same permeability testing procedure. During the tests, potential errors in the permeability measurements may arise from gas adsorption-induced deformations that are not fully recovered after vacuum, as well as irreversible deformations caused by repeated loading–unload-

Table 1
Initial permeability of cubic samples using helium gas.

Sample number	k_A (mD)	k_B (mD)	k_C (mD)	k_0 (mD)
S1	1.76	1.38	1.64	1.76
S2	2.59	1.92	2.00	2.59
S3	3.03	3.81	4.12	4.12
S4	8.20	4.81	4.17	8.20
S5	9.70	9.89	5.15	9.89
S6	15.18	10.30	2.55	15.18
S7	17.38	5.69	14.76	17.38
S8	29.28	13.73	8.84	29.28

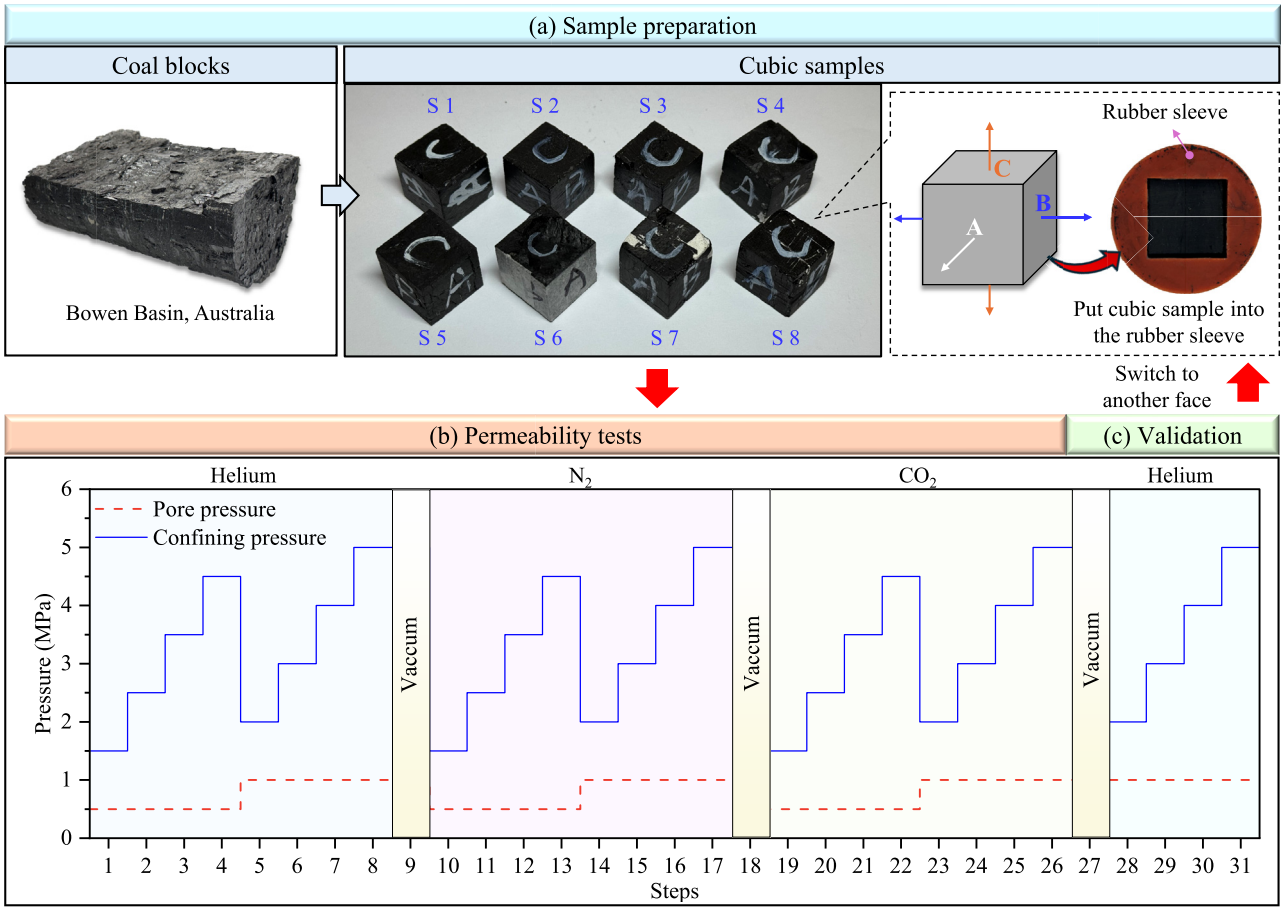

Fig. 3. Experimental procedure flowchart.

ing cycles. Therefore, after the final direction was tested, the sample was vacuumed again, and a repeatability test was conducted using helium to validate the reliability and repeatability of results. A brief experiment procedure is illustrated in Fig. 3.

2.4. Permeability measurement

The pressure transient method was used to conduct permeability tests in this work [39]. This method involves observing the decay in the differential pressure between the upstream and downstream cylinders across the sample. The pressure decay, along with the cylinder volumes, is used in the analysis to relate the flow through the sample and determine its permeability [40]. The pressure decay curve can be modelled according to previous work [41]:

$$\frac{P_{up}-P_{down}}{P_{up,0}-P_{down,0}}=e^{-m\times t} \tag{1}$$

where P_{up}–P_{down} is the pressure difference between the upstream and downstream cylinders used during the permeability test; $P_{up,0}$–$P_{down,0}$ the pressure difference between the upstream and downstream cylinders at the beginning of the test (ranges from 100 to 200 kPa in this work); and t the time and m is described below [41,42]:

$$m=\frac{k}{\mu C_g L^2}\times V_R\times\left(\frac{1}{V_{up}}+\frac{1}{V_{down}}\right) \tag{2}$$

where k is permeability; μ the viscosity; C_g the gas compressibility; L the sample length; V_R the sample volume; and V_{up} and V_{down} the volumes of the upstream and downstream cylinders (both are 75 mL in this work).

Above all, the permeability can be obtained by Eq. (2) after m is obtained from the pressure decay curve.

2.5. Repeatability testing and data validation

In this paper, the repeatability error (ε_{re}) was introduced to quantify the repeatability of the measured permeability data. The ε_{re} is defined as:

$$\varepsilon_{re}=\frac{|k_t-k_v|}{k_{avg}}\times 100\% \tag{3}$$

$$k_{avg}=\frac{k_t+k_v}{2} \tag{4}$$

where k_t is permeability measured during tests in Fig. 3b; k_v permeability measured during validation in Fig. 3c; and k_{avg} the average permeability of the two steps.

The permeability data and repeatability error were plotted in Fig. 4. The results show that most repeatability errors are well below 7%, having negligible impact on the overall fitting curve, which demonstrates the high reliability of the permeability data in this work.

3. Results and analysis

3.1. Evolution of coal permeability anisotropy with effective stress

3.1.1. Apparent permeability using non-absorbing helium gas

The apparent permeability results of coal samples measured using helium gas under varying effective stress are plotted in Fig. 5. It demonstrates that all coal samples exhibit pronounced permeability anisotropy. With increasing effective stress, permeability in different directions gradually decreases and values tend to converge, but anisotropy remains. In addition, under constant effective stress conditions, a rise in pore pressure leads to a reduction in apparent permeability. This behavior is attributed to the effective stress coefficient (ESC) typically being less than 1.0 in porous rock (e.g. coal and sandstone) [41]. For porous rocks, the law of effective stress can be expressed as [43]:

$$\sigma_e=\sigma_t-\alpha P_p \tag{5}$$

where σ_e is the effective stress; σ_t the total stress, α the effective stress coefficient; and P_p the pore pressure.

In laboratory tests, ESC is assumed to be 1.0 [30], and the same assumption is adopted in this work. However, this assumption may result in an underestimation of the effective stress when pore pressure increases, since the actual ESC is slightly less than 1.0 [44,45]. Consequently, under the same nominal effective stress, an increase in pore pressure can lead to a decrease in apparent permeability.

3.1.2. Apparent permeability using absorbing N_2 and CO_2

The apparent permeability under varying effective stress, measured separately using N_2 and CO_2, are shown in Figs. 6 and 7, respectively. Compared to non-absorbing helium, gas adsorption leads to a reduction in apparent permeability in all three directions

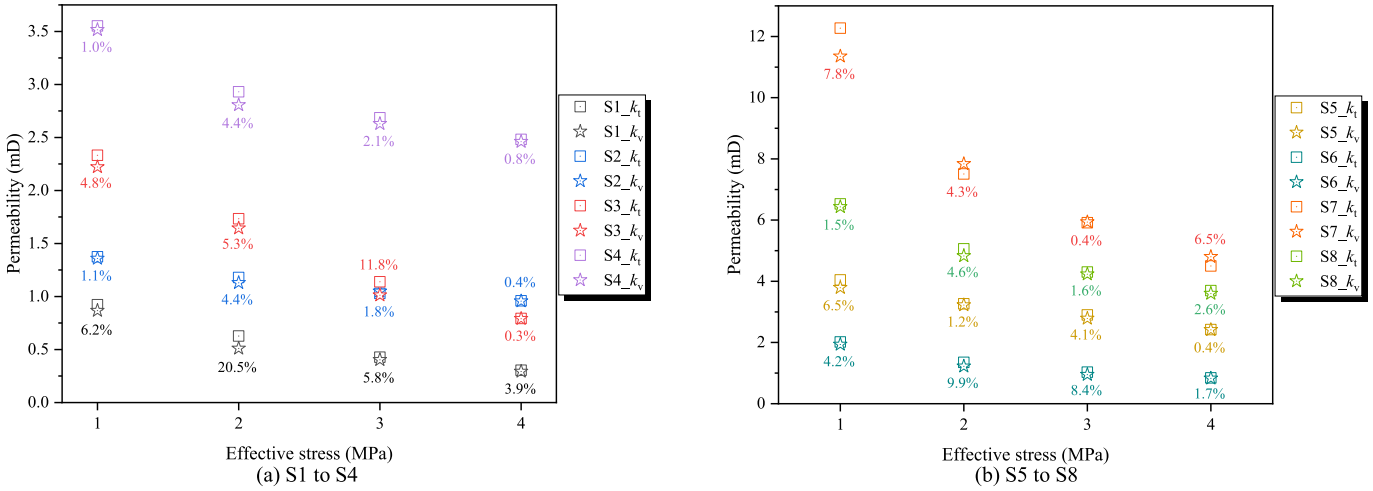

Fig. 4. Permeability data and repeatability error of all samples.

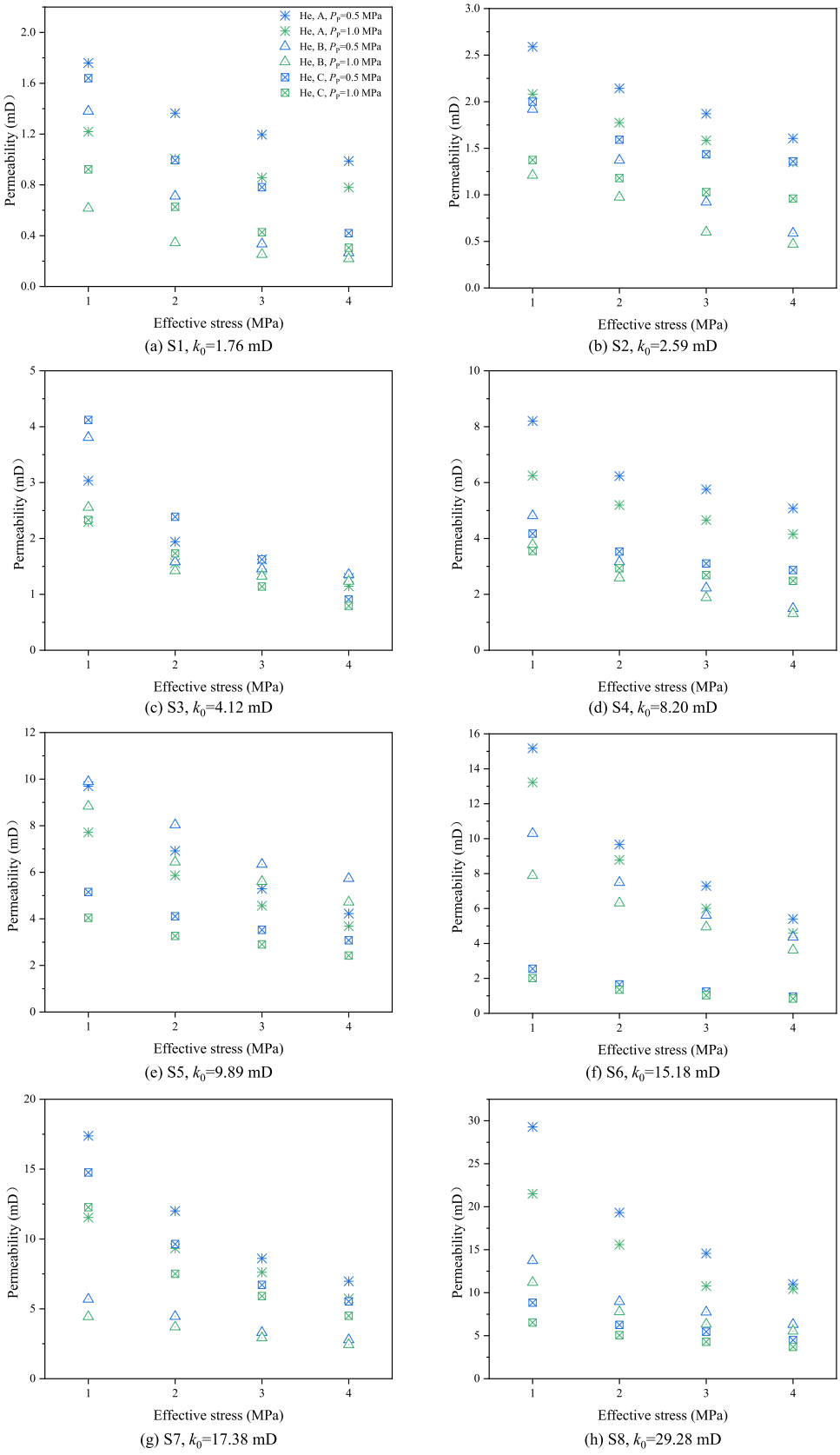

Fig. 5. Directional permeability variation of coal under different effective stresses.

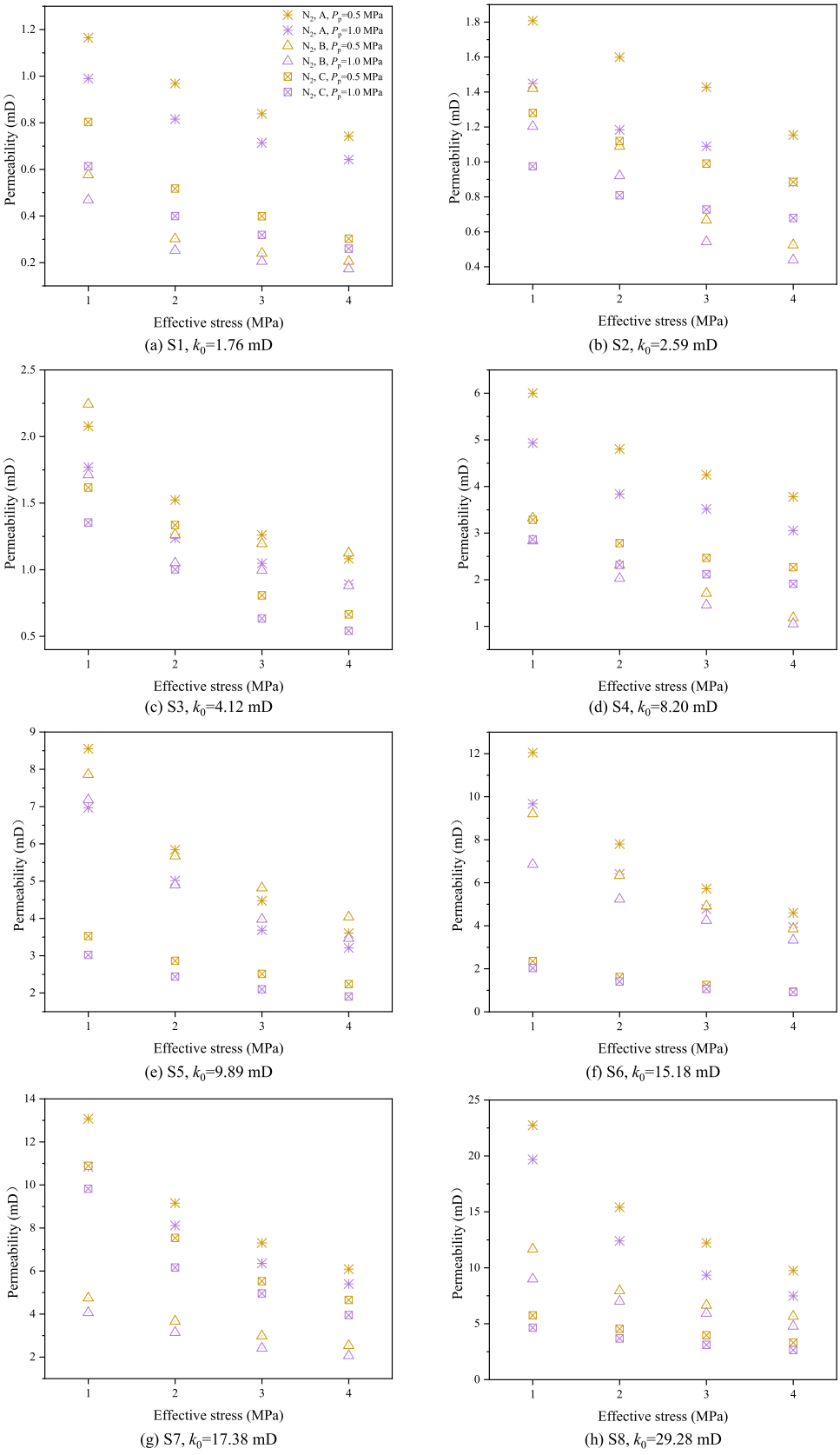

(a) S1, k_0=1.76 mD (b) S2, k_0=2.59 mD

(c) S3, k_0=4.12 mD (d) S4, k_0=8.20 mD

(e) S5, k_0=9.89 mD (f) S6, k_0=15.18 mD

(g) S7, k_0=17.38 mD (h) S8, k_0=29.28 mD

Fig. 6. Directional permeability variation of coal under different effective stresses using N_2.

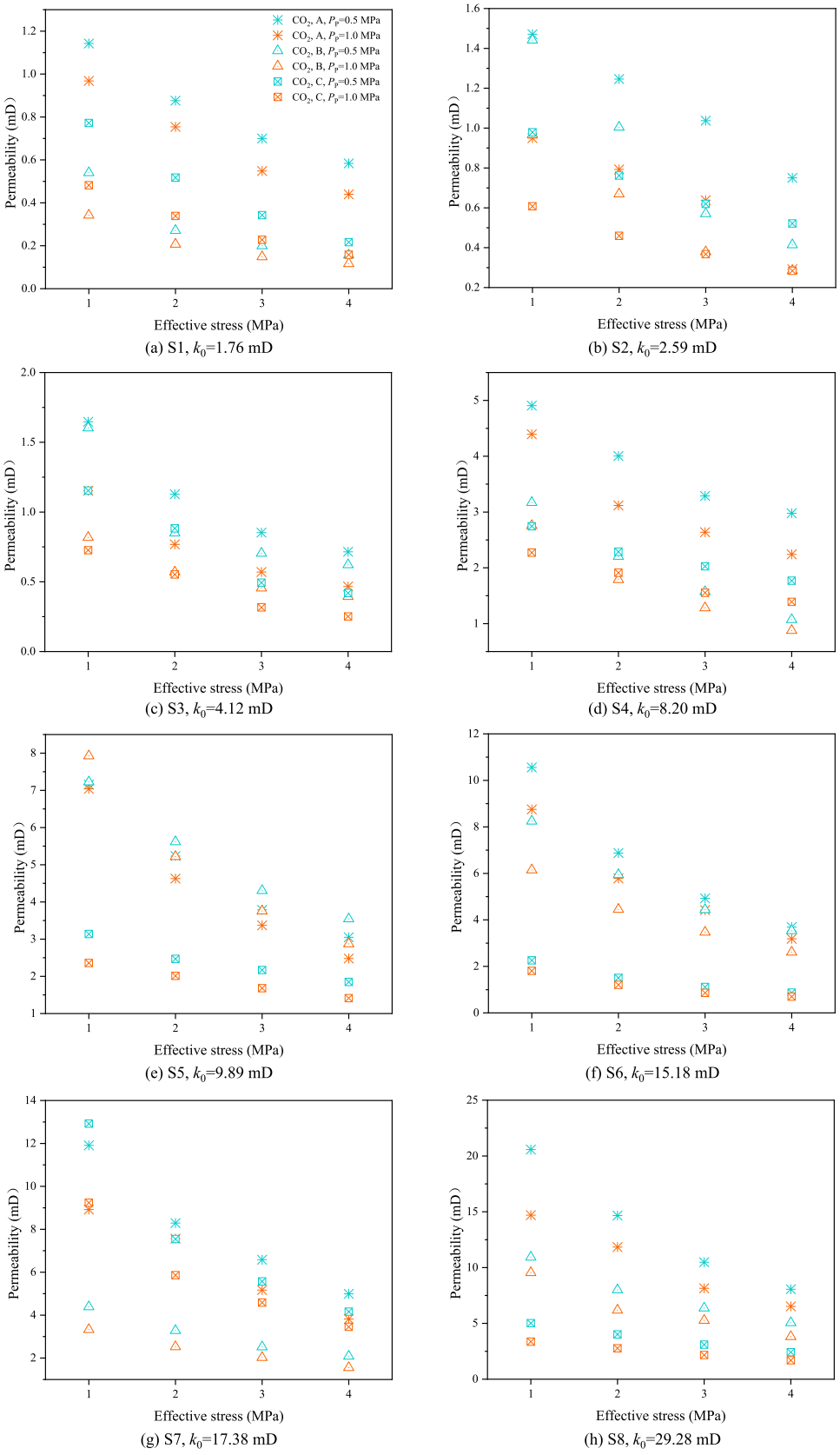

Fig. 7. Directional permeability variation of coal under different effective stresses using CO_2.

due to sorption-induced coal matrix swelling, although noticeable anisotropy still persists. Moreover, under the same effective stress, a rise in pore pressure leads to a reduction in apparent permeability. This behavior is the combined result of both the effective stress coefficient being less than 1.0 and the enhancement of gas adsorption [46].

3.2. Evolution of anisotropy ratio

3.2.1. Anisotropy ratio evolution with helium gas injection (effective stress impact)

In this section, data acquired from permeability tests using He are employed to analyze the impact of effective stress on coal anisotropy. To quantify the anisotropy of the coal samples, the anisotropy ratio (R) is defined as [32]:

$$R = \frac{k_{max}}{k_{min}} \tag{6}$$

where k_{max} is the maximum permeability; and k_{min} the minimum permeability among the three directions under the same stress conditions.

The variation of R with effective stress for the eight tested samples is shown in Fig. 8, with each color representing a sample with a different initial permeability (k_0). Results show that different coal samples exhibit varying permeability anisotropy ratios. Specifically, the anisotropy ratios range from 1.28 to 5.95 at a pore pressure of 0.5 MPa, and from 1.11 to 6.55 at 1.0 MPa. For each sample, the anisotropy ratio changes linearly with effective stress. The influence of effective stress on anisotropy ratio varies depending on the initial permeability. Specifically, for coal samples with high initial permeability, R decreases with increasing effective stress, whereas for those with low initial permeability, R tends to increase with increasing effective stress. Moreover, to establish a quantitative relationship between effective stress and R, we fitted R as a linear function of effective stress changes using Eqs. (7) and (8):

$$R = a \times \Delta\sigma_e + b \tag{7}$$

$$\Delta\sigma_e = \sigma_e - \sigma_{e0} \tag{8}$$

where $\Delta\sigma_e$ is the effective stress change; σ_{e0} the initial effective stress of 1 MPa for this work; and σ_e the effective stress; and a and b the fitting parameters.

The fitted dashed lines and corresponding results for He are presented in Fig. 8 and Table 2, respectively.

According to Table 2, the relationships between fitting parameters (a and b) and initial permeability (k_0) are plotted in Fig. 9. These figures demonstrate that both parameters a and b have a functional relationship with k_0. Above all, the relationships between anisotropy ratio (R), effective stress change ($\Delta\sigma_e$), and initial permeability (k_0) using helium gas (including two pore pressures) can be expressed as Eq. (9) according to Fig. 9c:

$$R = (-0.322 \times \ln k_0 + 0.782) \times \Delta\sigma_e + 0.073 \times k_0 + 1.273 \tag{9}$$

According to Eq. (9), the influence of increasing effective stress on the anisotropy ratio (R) is not consistent for coal samples with different k_0. A critical value of k_0 exists when fitting parameter a equals zero. When the initial permeability is lower than this critical value (11.32 mD for helium gas), the parameter a becomes positive, and R increases with increasing effective stress, indicating an enhancement of permeability anisotropy. In contrast, for coal samples with initial permeability exceed the critical value of k_0, the parameter a becomes negative, and increasing effective stress

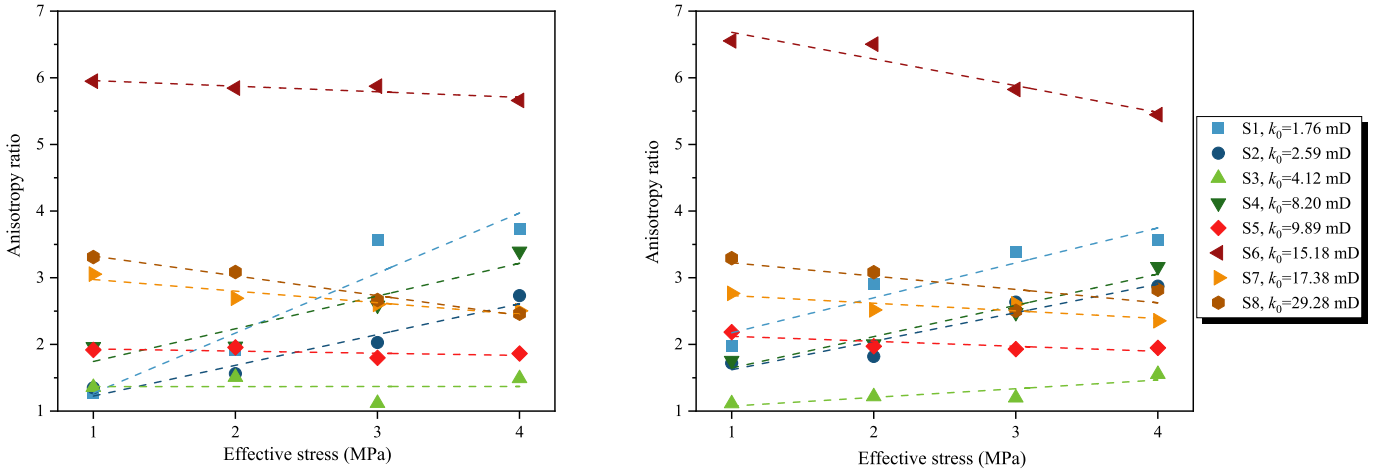

(a) He, P_{pore} = 0.5 MPa (b) He, P_{pore} = 1.0 MPa

Fig. 8. Anisotropy ratio (R) of coal samples under varying effective stresses (colors indicate different samples with varying initial permeabilities).

Table 2
Fitting parameters for linear relationship between $\Delta\sigma_e$ and R using helium gas.

Sample number	k_0 (mD)	P_{pore}=0.5 MPa			P_{pore}=1.0 MPa		
		A	B	R^2	A	b	R^2
S1	1.76	0.9003	1.2709	0.92	0.5243	2.1757	0.90
S2	2.59	0.4611	1.2266	0.95	0.4279	1.6209	0.91
S3	4.12	0.0009	1.3680		0.1303	1.0764	0.75
S4	8.20	0.4909	1.7450	0.88	0.4695	1.6483	0.96
S5	9.89	−0.0322	1.9332	0.37	−0.0750	2.1225	0.67
S6	15.18	−0.0839	5.9582	0.78	−0.4002	6.6823	0.92
S7	17.38	−0.1743	2.9750	0.88	−0.1145	2.7336	0.74
S8	29.28	−0.2969	3.3272	0.98	−0.2002	3.2262	0.57

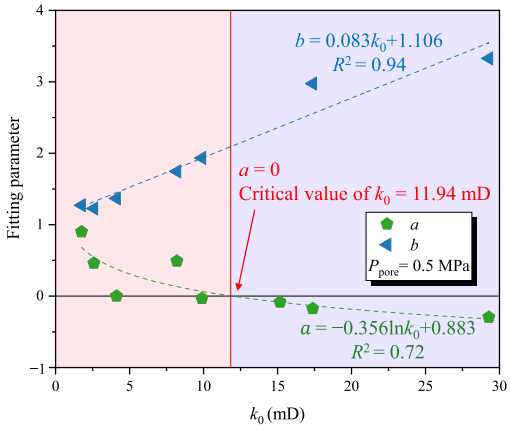

(a) Using He at a pore pressure of 0.5 MPa

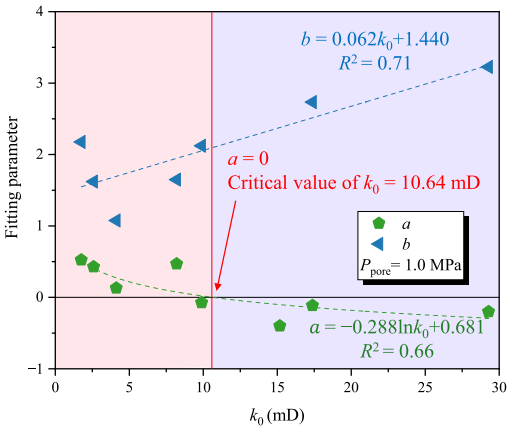

(b) Using He at a pore pressure of 1.0 MPa

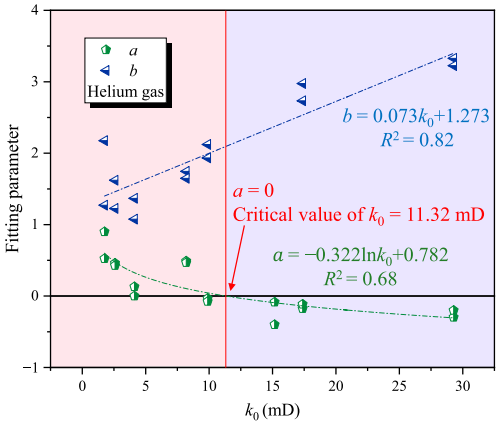

(c) Results for two pore pressures

Fig. 9. Fitting parameters a and b under different k_0 using He, and the critical value of k_0.

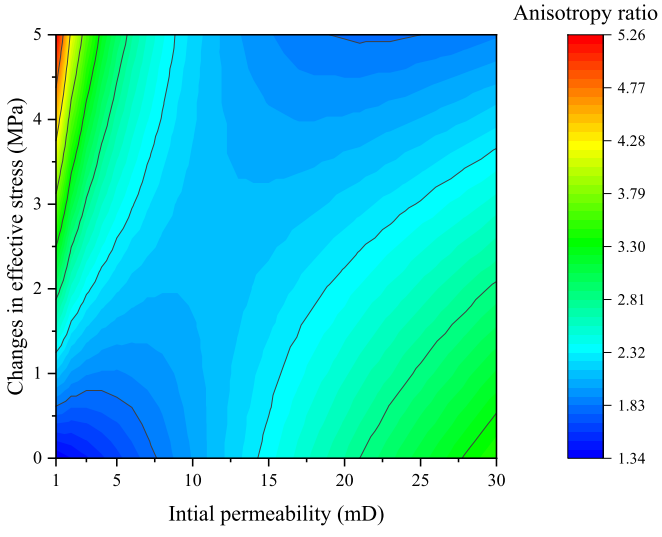

Fig. 10. Anisotropy ratio changes with k_0 and $\Delta\sigma_e$.

results in a decrease in R, suggesting a reduction in anisotropy. Moreover, coal samples with higher initial permeability (i.e., those with more extensively developed fracture networks) generally exhibit higher R.

To illustrate the impact of effective stress on the anisotropic permeability, the R values corresponding to different k_0 and effective stress ($\Delta\sigma_e$) were calculated using Eq. (9), shown in Fig. 10. It demonstrates that for coal samples with low k_0, increasing the effective stress leads to an increase in R, whereas for coal samples with high k_0, increasing the effective stress results in a decrease in R. In addition, coal samples with higher initial permeability tend to exhibit higher values of R. In summary, both k_0 and $\Delta\sigma_e$ have significant impact on coal anisotropic permeability.

3.2.2. Anisotropy ratio evolution with N_2 and CO_2 injection (adsorption impact)

In this section, data acquired from permeability tests using N_2 and CO_2 are employed to analyze the impact of adsorption on coal anisotropy. Similarly, based on the linear fitting using Eqs. (7) and (8), the fitted dashed lines and corresponding results for N_2 and CO_2 are summarized in Fig. 11, and Tables 3 and 4.

The results show that, under the effective stress of 1.0 MPa, the anisotropy ratios for N_2 range from 1.39 to 5.11 at a pore pressure of 0.5 MPa, and from 1.31 to 4.75 at 1.0 MPa. Correspondingly, for CO_2, the anisotropy ratios range from 1.43 to 4.68 at a pore pressure of 0.5 MPa, and from 1.59 to 4.85 at 1.0 MPa. In addition, it indicates the anisotropy ratio also changes linearly with effective stress when using N_2 and CO_2. Similar trends were observed in the N_2 and CO_2 tests as in the He tests. In both cases, R decreases with increasing effective stress for coal samples with high initial permeability, while increasing for those with low initial permeability.

Similarly, the relationships between fitting parameters (a and b) and initial permeability (k_0) for N_2 and CO_2 are plotted in Figs. 12

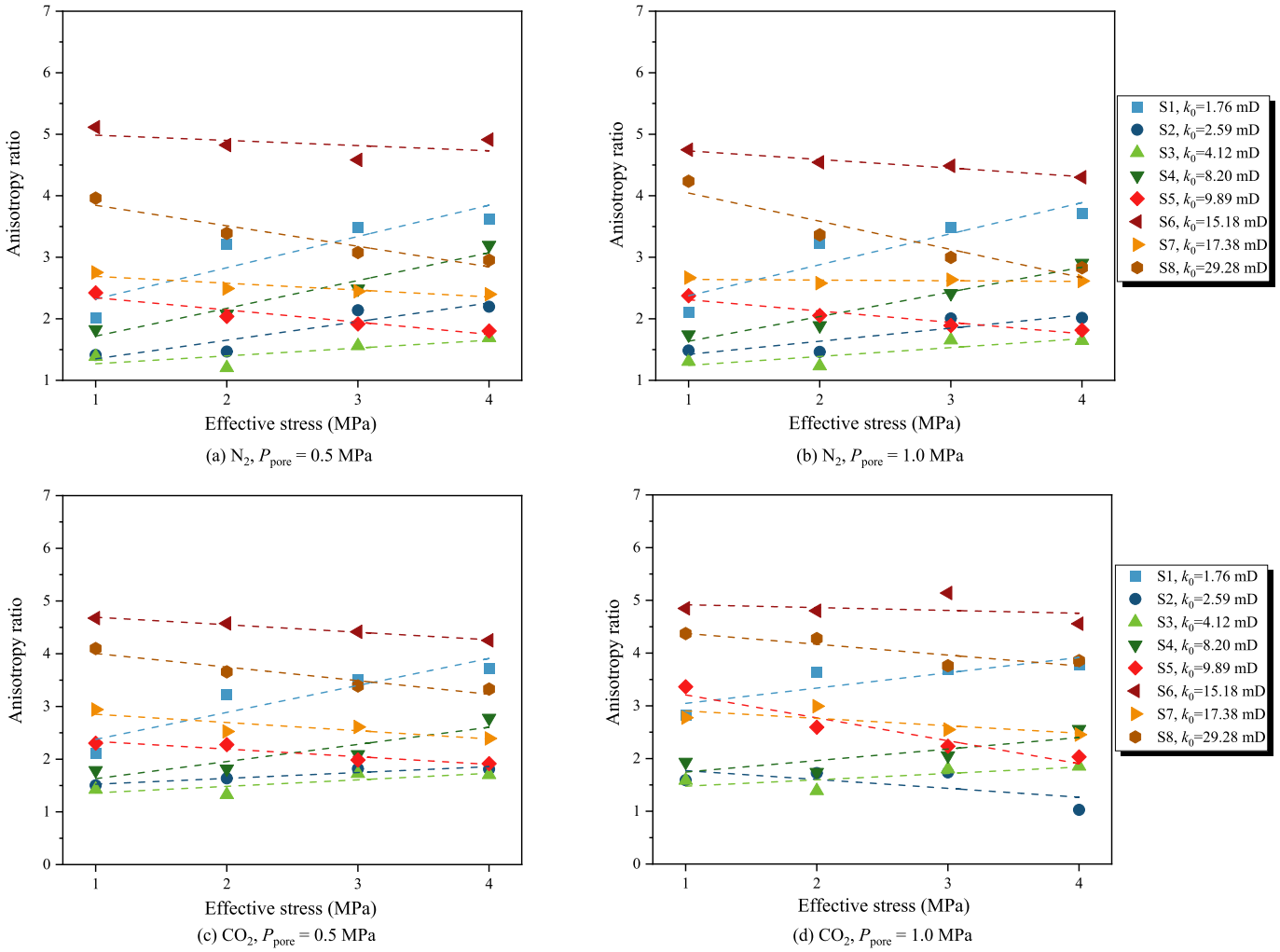

Fig. 11. Anisotropy ratio (R) of coal samples under varying effective stresses using N_2 and CO_2 (colors indicate different samples with varying initial permeabilities).

Table 3
Fitting parameters for linear relationship between $\Delta\sigma_e$ and R using N_2

Sample number	k_0 (mD)	P_{pore}=0.5 MPa			P_{pore}=1.0 MPa		
		a	B	R^2	a	b	R^2
S1	1.76	0.5081	2.3229	0.81	0.5041	2.3763	0.84
S2	2.59	0.3026	1.3505	0.86	0.2133	1.4228	0.79
S3	4.12	0.1275	1.2708	0.60	0.1441	1.2449	0.70
S4	8.20	0.4519	1.7197	0.95	0.4013	1.6364	0.96
S5	9.89	−0.1984	2.3440	0.90	−0.1842	2.3112	0.92
S6	15.18	−0.0847	4.9856	0.25	0.1395	4.7296	0.96
S7	17.38	−0.1110	2.6905	0.82	−0.0109	2.6414	0.14
S8	29.28	−0.3332	3.8461	0.92	−0.4583	4.0455	0.89

Table 4
Fitting parameters for linear relationship between $\Delta\sigma_e$ and R using CO_2.

Sample number	k_0 (mD)	P_{pore}=0.5 MPa			P_{pore}=1.0 MPa		
		a	B	R^2	a	b	R^2
S1	1.76	0.5114	2.3768	0.85	0.2899	3.0476	0.72
S2	2.59	0.1109	1.5260	0.89	−0.1680	1.7724	0.42
S3	4.12	0.1235	1.3619	0.63	0.1211	1.4768	0.54
S4	8.20	0.3251	1.6311	0.83	0.2180	1.7452	0.66
S5	9.89	−0.1451	2.3378	0.90	−0.4346	3.2079	0.92
S6	15.18	−0.1422	4.6930	0.99	−0.0535	4.9169	
S7	17.38	−0.1560	2.8528	0.74	−0.1407	2.9044	0.57
S8	29.28	−0.2575	4.0055	0.90	−0.2055	4.3741	0.77

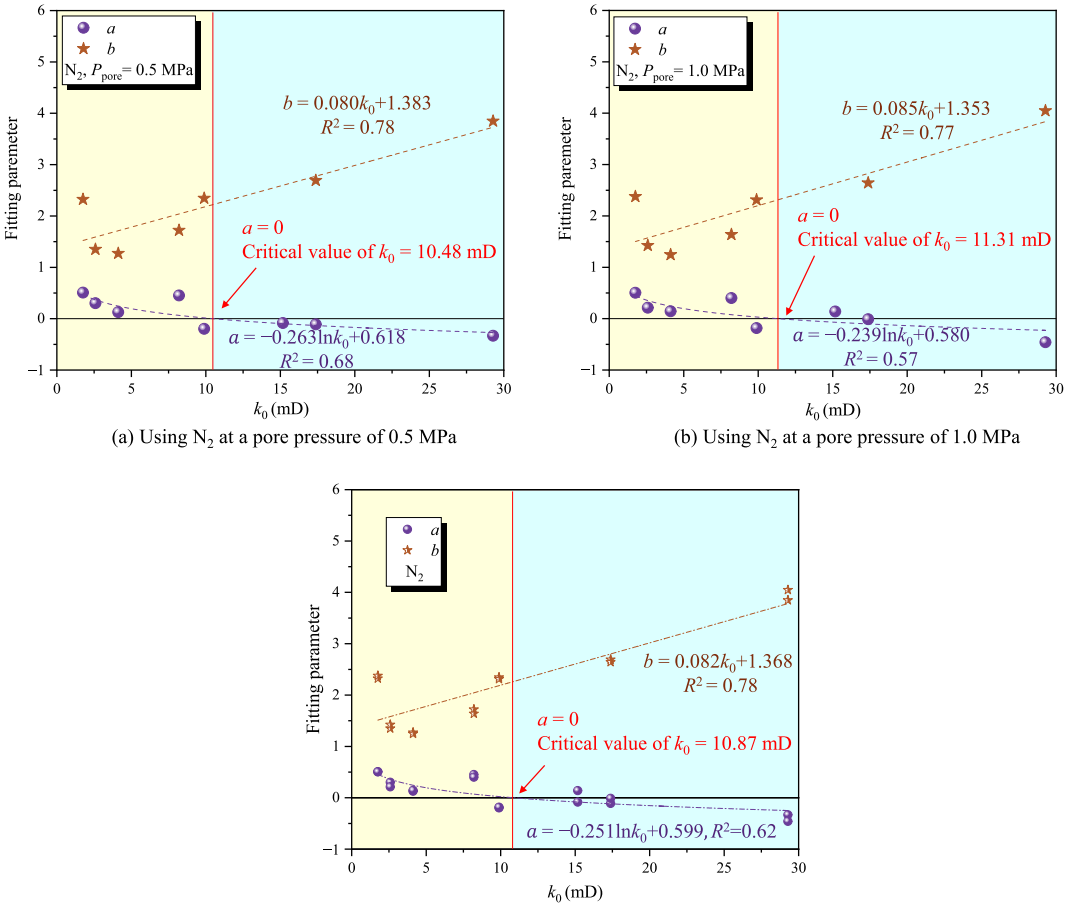

(a) Using N_2 at a pore pressure of 0.5 MPa

(b) Using N_2 at a pore pressure of 1.0 MPa

(c) Results for two pore pressures

Fig. 12. Fitting parameters a and b under different k_0 using N_2, and the critical value of k_0.

and 13, respectively. These figures also indicate that parameter a and b vary as a function of k_0. Furthermore, the relationships between anisotropy ratio (R), effective stress change ($\Delta\sigma_e$), and k_0 for adsorbing gases (i.e. N_2 and CO_2) are expressed as Eqs. (10) and (11) according to Figs. 12c and 13:

For N_2:

$$R = (-0.251 \times \ln k_0 + 0.599) \times \Delta\sigma_e + 0.082 \times k_0 + 1.368 \quad (10)$$

For CO_2:

$$R = (-0.177 \times \ln k_0 + 0.359) \times \Delta\sigma_e + 0.082 \times k_0 + 1.629 \quad (11)$$

A similar trend to that observed for helium gas was identified for the adsorbing gases (e.g., N_2 and CO_2), where the influence of increasing effective stress on the anisotropy ratio also depended on the initial permeability. In both cases, a critical value of k_0 exists at which the fitting parameter a equals zero. Specifically, for N_2 and CO_2, R increased with effective stress when the initial permeability was below the critical value of k_0 (10.87 mD for N_2 and 7.60 mD for CO_2), whereas it decreased when the initial permeability exceeded the threshold.

Above all, whether R decreases or increases with increasing effective stress depends on whether the initial permeability exceeds the critical value of k_0. However, the critical values differ among the three gases, as shown in Table 5. It indicates that when tested with adsorbing gases, coal samples exhibit lower critical values of k_0. Specifically, under the impact of gas adsorption, coal samples tend to exhibit a decrease in the anisotropy ratio (R) with increasing effective stress.

To illustrate the effect of gas adsorption on the anisotropic permeability, the R values corresponding to different k_0 under the condition of no effective stress change were calculated using Eqs. (9)–(11) for different gases and are plotted in Fig. 14. The results indicate that gas adsorption leads to an increase in anisotropy ratio. Specifically, at a k_0 of 5 mD, the anisotropy ratios are 1.64 for helium, 1.78 for N_2, and 2.04 for CO_2; while at 15 mD, the anisotropy ratios increase to 2.37, 2.60, and 2.86, respectively. This phenomenon can be attributed to the variation in cleat (or fracture) equivalent aperture induced by gas adsorption. Specifically, gas molecules adsorbed on the internal surfaces of micropores induce coal matrix swelling, which reduces pore throat size and narrows cleat apertures. Due to the heterogeneous distribution of pores and cleats, this swelling effect results in anisotropic permeability changes, with different degrees of reduction along the three flow directions. Low-permeability cleats exhibit higher adsorption sensitivity and therefore undergo more pronounced permeability reduction, whereas high-permeability cleats experience less reduction due to their lower sensitivity to adsorption-induced swelling [9]. Consequently, gas adsorption may lead to an increase in permeability anisotropy, which has also been reported in previous studies [47].

3.3. Degree of anisotropy

To quantify the degree of permeability anisotropy, an equivalent permeability is introduced to represent the permeability of the sample under the assumption of isotropy [31], as defined in Eq. (12):

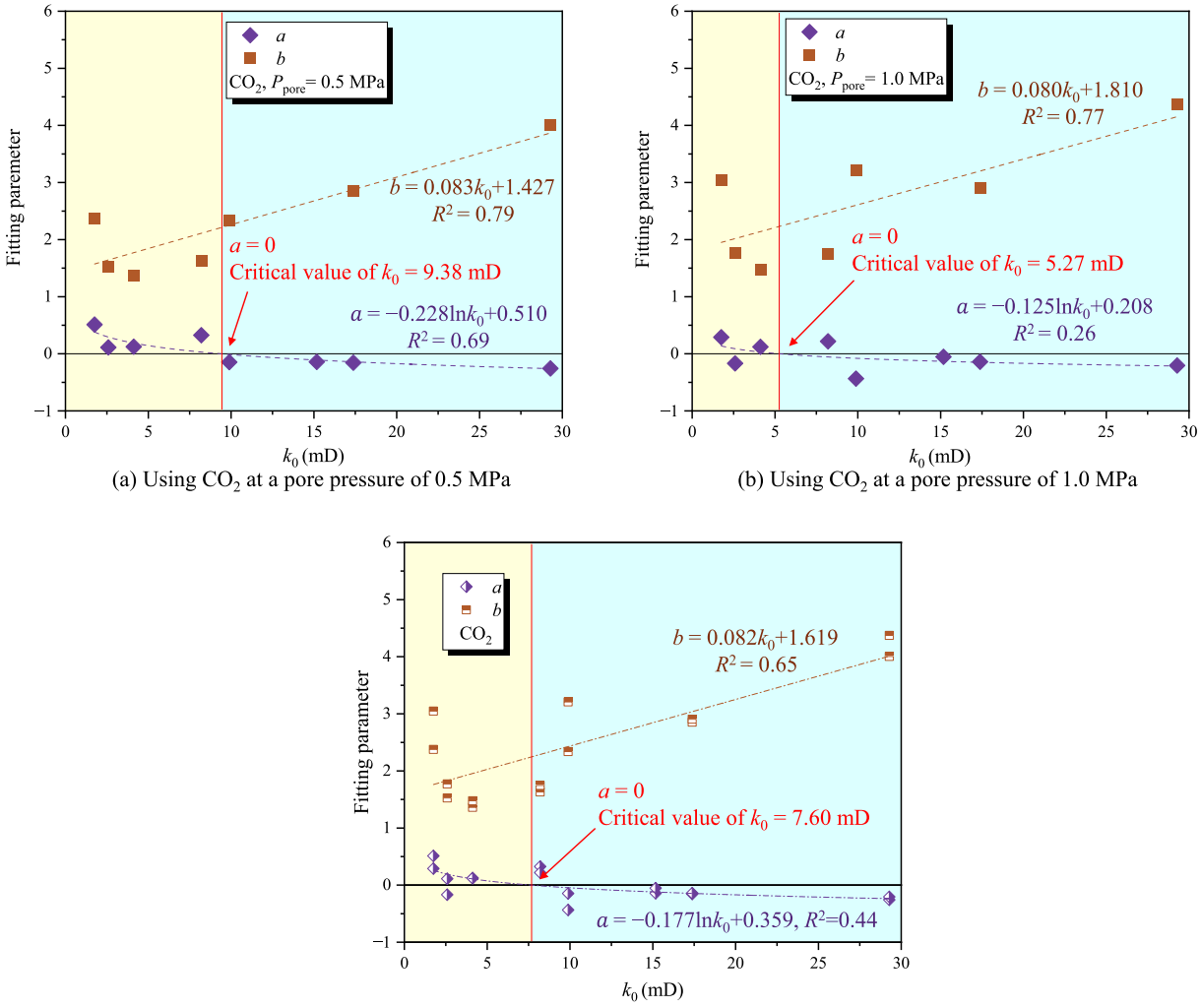

(a) Using CO_2 at a pore pressure of 0.5 MPa

(b) Using CO_2 at a pore pressure of 1.0 MPa

(c) Results for two pore pressures

Fig. 13. Fitting parameters a and b under different k_0 using CO_2, and the critical value of k_0.

Table 5
Critical values of k_0 under different gases.

Gas type	Critical value of k_0 (mD)
He	11.32
N_2	10.87
CO_2	7.60

$$k_{iso} = (k_A \times k_B \times k_C)^{\frac{1}{3}} \tag{12}$$

where k_{iso} is the equivalent permeability; k_A, k_B and k_C the permeabilities measured in A, B and C directions at the same stress conditions, respectively.

Furthermore, the degree of anisotropy is quantified by the quadratic deviation I of the permeability tensor from k_{iso} [31]:

$$I = \sqrt{\frac{(k_A - k_{iso})^2 + (k_B - k_{iso})^2 + (k_C - k_{iso})^2}{k_A^2 + k_B^2 + k_C^2}} \tag{13}$$

where I is the deviation from isotropy, expressed as a percentage, ranging from 0 to 100%. The closer I is to 100%, the greater the degree of anisotropy. When I=0, the material is isotropic.

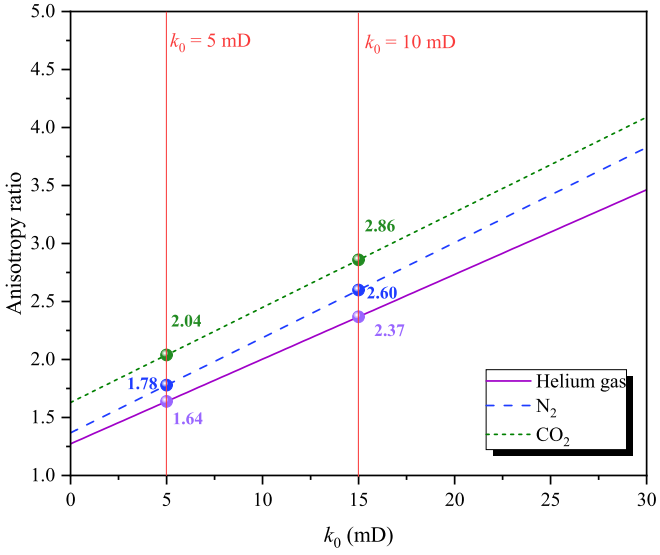

Fig. 14. Anisotropy ratio changes with gas type and k_0.

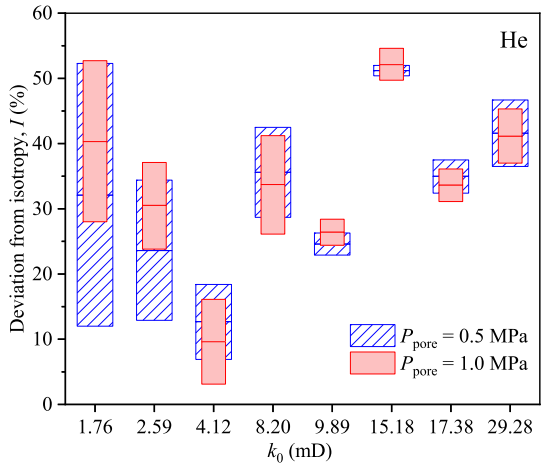

Fig. 15. Degree of anisotropy (I) of coal under different k_0 using He.

The deviation from isotropy (I) varies as the effective stress increases from 1.0 to 4.0 MPa, and the corresponding variation range is illustrated by the bars in Figs. 15 and 16. The results demonstrate that pore pressure has a limited influence on the degree of anisotropy. However, as k_0 increased, the variation range of I gradually decreased as effective stress changes from 1 to 4 MPa, which was reflected by the shortening of the bars from left to right. In other words, for coal samples with well-developed cleat networks, the impact of changing effective stress on anisotropy degree becomes less pronounced.

3.4. Cleat compressibility

3.4.1. Influence of initial permeability

Although the apparent permeability of coal exhibits significant anisotropy, whether the cleat compressibility (C_f) is anisotropic remains unclear due to the lack of direct experimental evidence. To investigate this issue, C_f was derived from the apparent

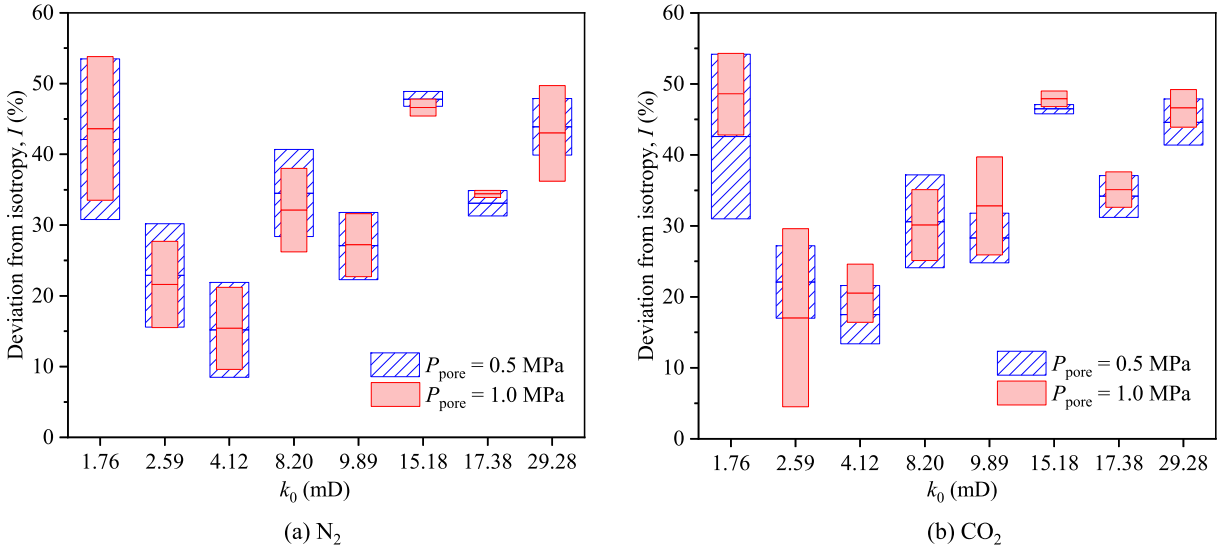

Fig. 16. Degree of anisotropy (I) of coal under different k_0 using N_2 and CO_2.

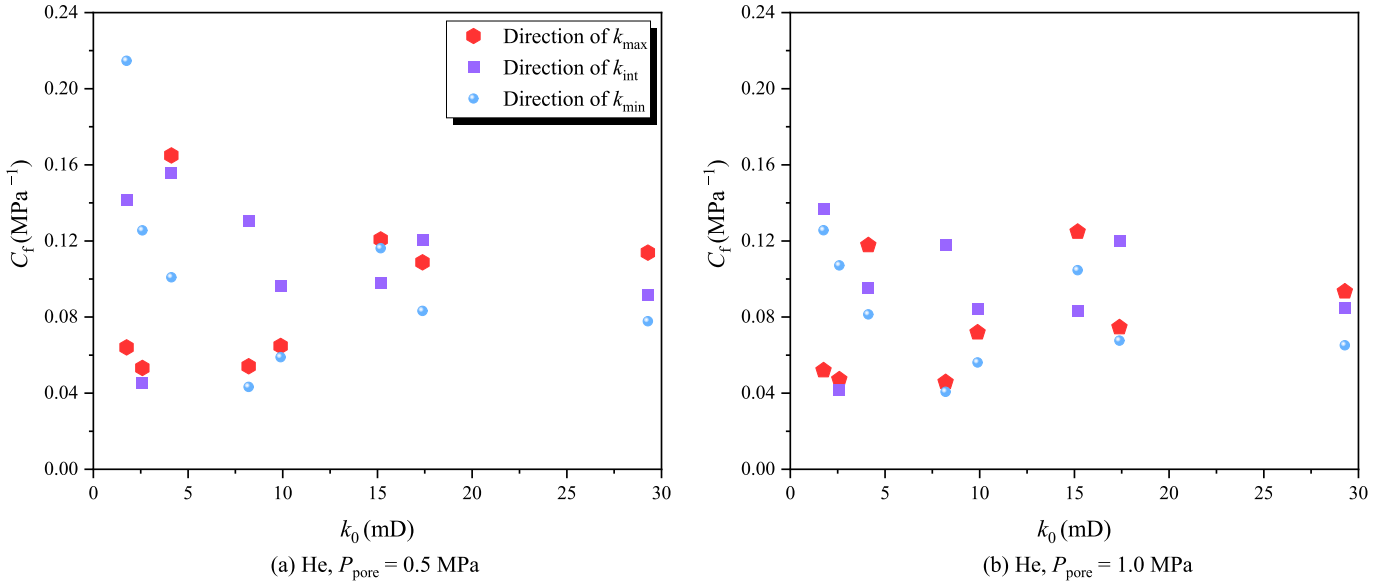

Fig. 17. Anisotropy of compressibility coefficients of coal samples.
Note: Directions of k_{max}, k_{int}, and k_{min} correspond to the maximum, intermediate, and minimum permeability directions of each sample, respectively.

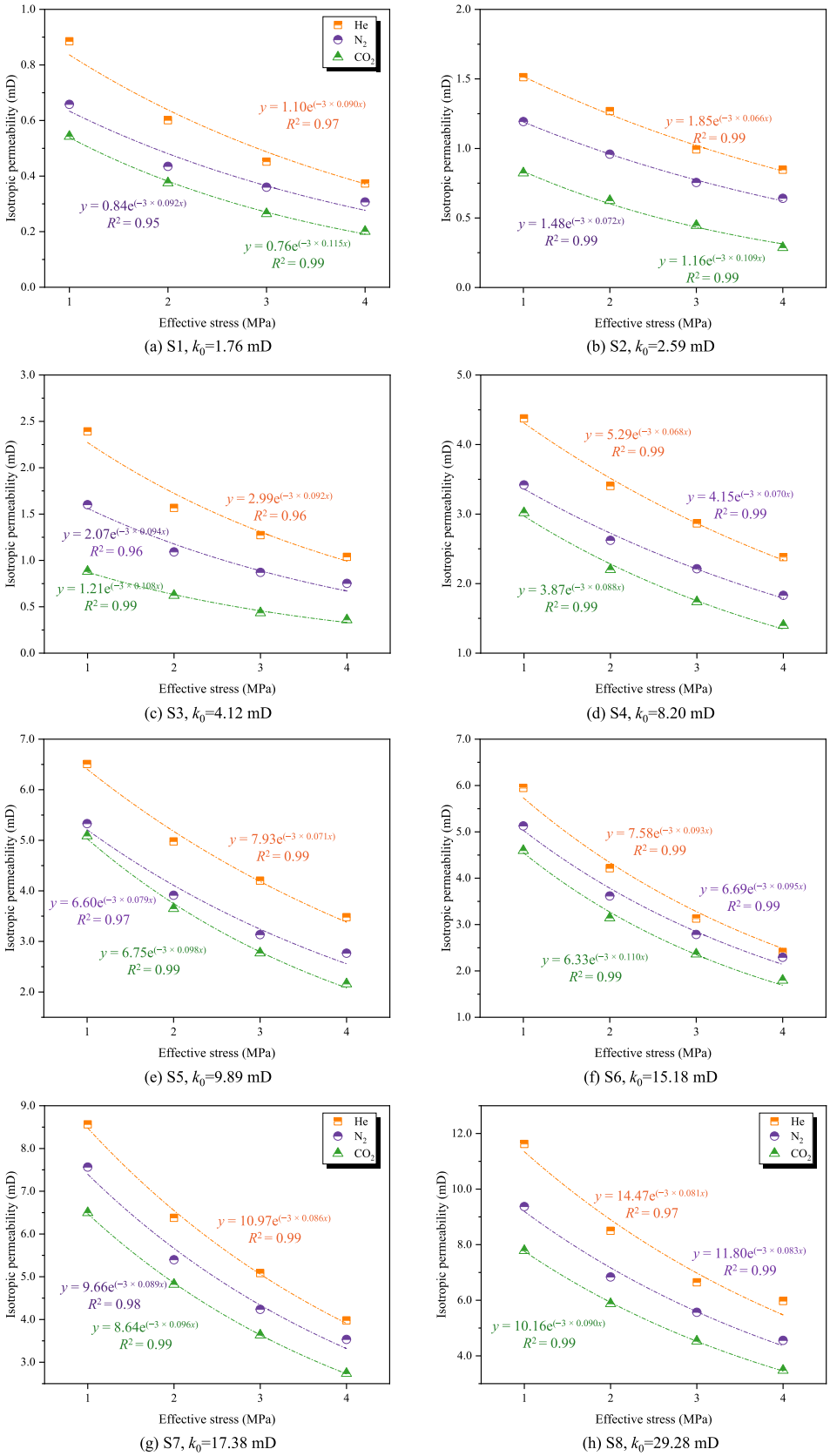

(a) S1, k_0=1.76 mD (b) S2, k_0=2.59 mD

(c) S3, k_0=4.12 mD (d) S4, k_0=8.20 mD

(e) S5, k_0=9.89 mD (f) S6, k_0=15.18 mD

(g) S7, k_0=17.38 mD (h) S8, k_0=29.28 mD

Fig. 18. Isotropic permeability variation of coal under different effective stresses and gases.

permeability data measured by helium gas (Fig. 5), as calculated by the following empirical equation [48]:

$$k_2 = k_1 \exp(-3C_f \times \Delta\sigma_e) \quad (14)$$

where k_2 is the permeability at effective stress of σ_{e2}; k_1 the permeability at the effective stress of σ_{e1}; C_f the cleat compressibility; and $\Delta\sigma_e$=σ_{e2}−σ_{e1} the effective stress change.

The cleat compressibility (C_f) of three directions for each sample is shown in Fig. 17. The results reveal that C_f also exhibits significant anisotropy, and the direction with the largest permeability does not always have the highest C_f [30]. In addition, with increasing initial permeability, implying more developed fracture networks, the C_f in different directions gradually become more uniform. Overall, pore pressure shows a limited influence on the C_f values.

3.4.2. Influence of gas adsorption

To evaluate the influence of gas adsorption on cleat compressibility, the equivalent permeability (k_{iso}) under a pore pressure of 1.0 MPa, as calculated from Eq. (12), was selected for comparison. Furthermore, Eq. (14) was used to fit the relationship between k_{iso} and effective stress, as shown in Fig. 18. It can be observed that the k_{iso} decreased with increasing effective stress, and the fitting results exhibited a good agreement with the experimental data [49].

The C_f values derived from the fitting results are plotted in Fig. 19. It illustrates that gas adsorption has a noticeable impact on C_f, leading to an increase in C_f, especially for CO_2. This phenomenon is attributed to gas adsorption. When gas molecules, particularly CO_2, are adsorbed onto the internal surfaces of coal micropores and the matrix, they cause the coal to swell. This swelling not only reduces the size of pore throats and cleat apertures but also lowers the elastic modulus of coal [50], effectively softening the matrix. As a result, the cleats become more compressible under the same external stress, leading to an increase in the cleat compressibility. This mechanism also accounts for the more pronounced increase in C_f for CO_2 compared to gases with lower adsorption affinity, such as N_2 [51,52].

4. Conclusions and recommendations

In this work, more than 600 permeability tests were performed on eight cubic coal samples from Bowen Basin, Australia, to investigate the impact of effective stress and gas adsorption on the evolution of coal permeability anisotropy ratio. The reliability of the experimental data was verified through repeatability testing. The primary conclusions are as follows:

(1) Anisotropy magnitude: All cubic coal samples exhibited pronounced permeability anisotropy, with ratios ranging from 1.11 to 6.55. While permeability in all directions decreased with increasing effective stress, anisotropy remained evident. The anisotropy magnitude was found to be dynamic rather than constant, highlighting the need to consider effective stress changes and gas adsorption when evaluating anisotropic permeability.
(2) Anisotropy ratio: Our results reveal that the evolution of the anisotropy ratio is strongly controlled by effective stress, initial permeability and gas adsorption. Specifically, when the initial permeability was below a critical permeability value, the anisotropy ratio increases with increasing effective stress, reflecting an enhancement of permeability anisotropy. Above the critical value, the anisotropy ratio decreases with increasing effective stress. However, under the impact of gas adsorption, coal samples exhibit lower critical values. Based on these observations, quantitative relationships between the anisotropy ratio, effective stress, and initial permeability were established for helium, N_2 and CO_2, respectively.
(3) Degree of anisotropy: The results show that pore pressure has a limited impact on the degree of anisotropy. However, as the initial permeability increased, the variation range of anisotropy degree gradually decreased when increasing effective stress. In other words, for coal samples with well-developed cleat networks, changes in effective stress have a less pronounced impact on anisotropy degree.
(4) Anisotropy of cleat compressibility: The cleat compressibility of coal also exhibited notable anisotropy, and the direction with the highest permeability did not necessarily correspond to the largest cleat compressibility. As the initial permeability increased, indicating better-developed fracture networks, the differences in cleat compressibility among the three directions tended to diminish. Moreover, gas adsorption, especially CO_2, was found to enhance cleat compressibility, which may further weaken the coal structure and alter its mechanical behavior.

These findings suggest that field gas injection strategies should consider the evolution of permeability anisotropy when predicting injectivity and migration pathways of the injected gas. For example, during gas injection, the increase in pore pressure leads to a decrease in effective stress, which in turn alters the anisotropy ratio of coal permeability. Gas adsorption can further modify this stress-dependent anisotropy evolution, particularly for strongly adsorbing gases such as CO_2. Therefore, accounting for stress-induced and adsorption-induced anisotropy evolution is critical for injected gases migration prediction and injectivity management in both CO_2 geo-sequestration and compressed air energy storage projects.

Key recommendations for the future are as follows:

(1) Initial permeability range expansion: Although the initial permeability range of the coal samples selected in this study may represent the majority of coal seam permeabilities, future research should include investigations on low-permeability coal (e.g., permeability less than 0.1 mD) and high-permeability coal (e.g., initial permeability greater than 50 mD) to further complement and enhance the findings of this study.

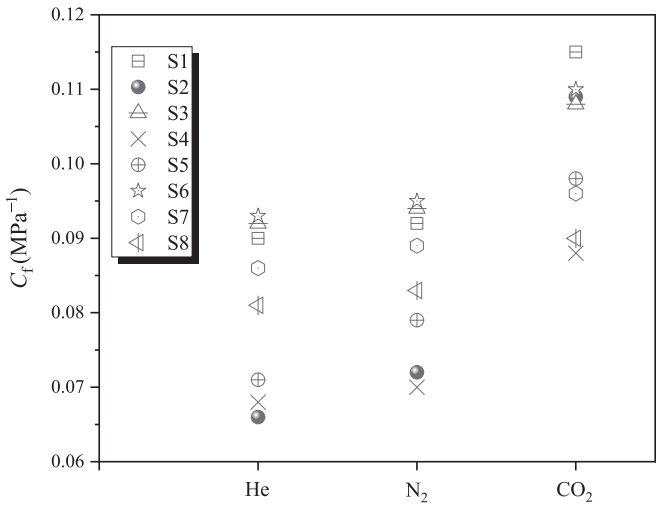

Fig. 19. Sample cleat compressibility (C_f) of different gases at a pore pressure of 1.0 MPa.

(2) Control of experimental errors: In this work, to minimize experimental errors, the samples were vacuumed after the adsorption tests to remove gas-induced swelling, and multiple cycles of confining pressure loading and unloading were applied to reduce the impact of irreversible deformation. However, it remains uncertain whether the experimental errors would increase with the number of repeated trials. Future experiments will further explore effective approaches for experimental error elimination.

(3) Generalizability of the quantitative relationships: The quantitative relationships derived in this study were established under the specific stress loading path of constant axial pressure with varying confining pressure. However, previous studies adopted different stress conditions, such as hydrostatic pressure, and thus no suitable data are currently available to validate our model. Further investigations are needed to test the robustness of the model under alternative loading paths, to validate its general applicability.

Acknowledgments

The project was partially funded by industry members APLNG, Arrow Energy, and Santos through The Gas and Energy Transition Research Centre in The University of Queensland. The information, opinions and views expressed in this presentation do not necessarily represent those of The University of Queensland, The UQ Gas and Energy Transition Research Centre or its constituent members or associated companies.

References

[1] Liu XD, Sang SX, Zhou XZ, Wang ZL. Coupled adsorption-hydro-thermo-mechanical-chemical modeling for CO_2 sequestration and well production during CO_2-ECBM. Energy 2023;262:125306.
[2] Schmidt F, Menéndez J, Konietzky H, Pascual-Muñoz P, Castro J, Loredo J, Bernardo Sánchez A. Converting closed mines into giant batteries: Effects of cyclic loading on the geomechanical performance of underground compressed air energy storage systems. J Energy Storage 2020;32:101882.
[3] Menéndez J, Ordóñez A, Rodrigo Á, Loredo J. Energy from closed mines: Underground energy storage and geothermal applications. Renew Sustain Energy Rev 2019;108:498–512.
[4] Wu QF, Yu MG. Effect of barrier hole shape on gas explosion behavior under non-uniform conditions. Fuel 2026;405:136464.
[5] Ran QC, Liang YP, Ye CF, Ning YH, Ma TF, Kong FJ. Failure analysis of overlying strata during inclined coal seam mining: Insights from acoustic emission monitoring. Eng Fail Anal 2025;182:110023.
[6] Li JH, Li BB, Cheng QY, Gao Z. Characterization of anisotropic coal permeability with the effect of sorption-induced deformation and stress. Fuel 2022;309:122089.
[7] Gao XY, Liu YJ, Zhang LM, Deng CB, Song LN, Zhang Y. Regulatory mechanism of microscopic pore structure on anisotropy of gas multimodal seepage in original coals. Energy 2024;300:131611.
[8] Ran QC, Zhao WT, Liang YP, Ye CF, Ning YH. Deciphering confining pressure effects on coal failure mechanisms using acoustic emission approaches. Eng Fract Mech 2025;329:111592.
[9] Chen M, Masum S, Sadasivam S, Thomas H. Modelling anisotropic adsorption-induced coal swelling and stress-dependent anisotropic permeability. Int J Rock Mech Min Sci 2022;153:105107.
[10] Yue GW, Liu H, Yue JW, Li MM, Liang WM. Influence radius of gas extraction borehole in an anisotropic coal seam: Underground in situ measurement and modeling. Energy Sci Eng 2019;7(3):694–709.
[11] Yan TH, Xu XM, Liu JF, Zhang YH, Arif M, Xu XW, Wang Q. Data-driven predictive model of coal permeability based on microscopic fracture structure characterization. J Rock Mech Geotech Eng 2025;17(7):4476–89.
[12] Liu A, Liu SM, Wang G, Sang GJ. Modeling of coal matrix apparent strains for sorbing gases using a transversely isotropic approach. Rock Mech Rock Eng 2020;53(9):4163–81.
[13] Zhang TC, Li JX, Zhu YR, Rudolph V, Chen ZW. Impact of gas adsorption on coal relative permeability: A laboratory study. Int J Rock Mech Min Sci 2025;194:106191.
[14] Ge ZL, Li CT, Zhou Z, Zhang XY, Guan YR, Sheng MY. Expansion deformation and permeability characteristics of bituminous coal with different moisture content after CO_2 adsorption. Geoenergy Sci Eng 2023;227:211828.
[15] Xiao ZY, Wang G, Wang CS, Jiang YJ, Jiang F, Zheng CC. Permeability evolution and gas flow in wet coal under non-equilibrium state: Considering both water swelling and process-based gas swelling. Int J Min Sci Technol 2023;33(5):585–99.
[16] Palmer I, Mansoori J. How permeability depends on stress and pore pressure in coalbeds: A new model. SPE Reserv Eval Eng 1998;1(6):539–44.
[17] Pan ZJ, Connell LD. A theoretical model for gas adsorption-induced coal swelling. Int J Coal Geol 2007;69(4):243–52.
[18] Shi JQ, Durucan S. Drawdown induced changes in permeability of coalbeds: A new interpretation of the reservoir response to primary recovery. Transp Porous Medium 2004;56(1):1–16.
[19] Liu SM, Wang Y, Harpalani S. Anisotropy characteristics of coal shrinkage/swelling and its impact on coal permeability evolution with CO_2 injection. Greenh Gases Sci Technol 2016;6(5):615–32.
[20] Espinoza DN, Vandamme M, Dangla P, Pereira JM, Vidal-Gilbert S. A transverse isotropic model for microporous solids: Application to coal matrix adsorption and swelling. J Geophys Res Solid Earth 2013;118(12):6113–23.
[21] Wu SW, Wang L, Liu C, Su S, Lu Z, He XX, Yang QL, Guo LW. Experimental study of deformation induced by high-pressure methane adsorption and desorption: Insights into anisotropy and hysteresis characteristics. Int J Rock Mech Min Sci 2025;186:106035.
[22] Zhang XY, Wu CF, Wang ZW, Zhou AT. Experimental study of the effective stress coefficient for coal permeability with different water saturations. J Petrol Sci Eng 2019;182:106282.
[23] Li JH, Li BB, Wang ZH, Ren CH, Yang K, Gao Z. A permeability model for anisotropic coal masses under different stress conditions. J Petrol Sci Eng 2021;198:108197.
[24] Snow DT. Anisotropic permeability of fractured media. Water Resour Res 1969;5(6):1273–89.
[25] Xiao K, Zhang ZT, Zhang R, Gao MZ, Xie J, Zhang AL, Liu Y. Anisotropy of the effective porosity and stress sensitivity of coal permeability considering natural fractures. Energy Rep 2021;7:3898–910.
[26] Lou Z, Wang K, Zang J, Zhao W, Qin BB, Kan T. Effects of permeability anisotropy on coal mine methane drainage performance. J Nat Gas Sci Eng 2021;86:103733.
[27] Yan Z, Wang K, Zang J, Wang C, Liu A. Anisotropic coal permeability and its stress sensitivity. Int J Min Sci Tech 2019;29(3):507–11.
[28] Duan MK, Jiang CB, Gan Q, Zhao HB, Yang Y, Li ZK. Study on permeability anisotropy of bedded coal under true triaxial stress and its application. Transp Porous Medium 2020;131(3):1007–35.
[29] Liu C, Yin GZ, Li MH, Shang DL, Deng BZ, Song ZL. Deformation and permeability evolution of coals considering the effect of beddings. Int J Rock Mech Min Sci 2019;117:49–62.
[30] Tan YL, Pan ZJ, Liu JS, Zhou FB, Connell LD, Sun WJ, Haque A. Experimental study of impact of anisotropy and heterogeneity on gas flow in coal. Part ii: Permeability. Fuel 2018;230:397–409.
[31] Clavaud JB, Maineult A, Zamora M, Rasolofosaon P, Schlitter C. Permeability anisotropy and its relations with porous medium structure. J Geophys Res Solid Earth 2008;113(B1):B01202.
[32] Armitage PJ, Faulkner DR, Worden RH, Aplin AC, Butcher AR, Iliffe J. Experimental measurement of, and controls on, permeability and permeability anisotropy of caprocks from the CO_2 storage project at the Krechba Field, Algeria. J Geophys Res Solid Earth 2011;116(B12):B12208.
[33] Li M, Ma YX, Kong XW, Xia ZH, Zhu HQ. Seismic application in Australia Bowen basin CBM well drilling and development well placement. In: Proceedings of the International Field Exploration and Development Conference 2018. Singapore: Springer Singapore; 2019.p.485–94.
[34] Kelloway SJ, Ward CR, Marjo CE, Wainwright IE, Cohen DR. Quantitative chemical profiling of coal using core-scanning X-ray fluorescence techniques. Int J Coal Geol 2014;128:55–67.
[35] Sander R, Pan ZJ, Connell LD. Laboratory measurement of low permeability unconventional gas reservoir rocks: A review of experimental methods. J Nat Gas Sci Eng 2017;37:248–79.
[36] Liu C, Zhang JH, Wu SW, Qi JH, Yu BC, Wang L. Experimental study on permeability evolution of deep high-stressed coal under major horizontal stress unloading paths. Int J Min Sci Technol 2024;34(11):1495–508.
[37] Zhang C, Zhang L, Wang W. The axial and radial permeability testing of coal under cyclic loading and unloading. Arab J Geosci 2019;12(11):371.
[38] Raza SS, Ge L, Rufford TE, Chen ZW, Rudolph V. Anisotropic coal permeability estimation by determining cleat compressibility using mercury intrusion porosimetry and stress-strain measurements. Int J Coal Geol 2019;205:75–86.
[39] Peng S. Evaluating the accuracy of liquid permeability measurements in shale and tight rocks using transient flow method and comparison with gas permeability. Mar Petrol Geol 2023;157:106491.
[40] Hildenbrand A, Schlömer S, Krooss BM. Gas breakthrough experiments on fine-grained sedimentary rocks. Geofluids 2002;2(1):3–23.
[41] Chen ZW, Pan ZJ, Liu JS, Connell LD, Elsworth D. Effect of the effective stress coefficient and sorption-induced strain on the evolution of coal permeability: Experimental observations. Int J Greenh Gas Contr 2011;5(5):1284–93.
[42] Zhao YY, Zhao YX, Wei MY, Liu JS, Cui DX. A new experimental system and method for periodically measuring permeability and strains of coal. Gas Sci Eng 2023;110:204909.
[43] Zhang K, Zhou H, Hu DW, Zhao Y, Feng XT. Theoretical model of effective stress coefficient for rock/soil-like porous materials. Acta Mech Solida Sin 2009;22(3):251–60.
[44] Lv A, Ali Aghighi M, Masoumi H, Roshan H. The effective stress coefficient of coal: A theoretical and experimental investigation. Rock Mech Rock Eng 2021;54(8):3891–907.

[45] Zhang XY, Wu CF, Wang ZW. Experimental study of the effective stress coefficient for coal permeability with different water saturations. J Petrol Sci Eng 2019;182:106282.
[46] Chen ZW, Liu JS, Pan ZJ, Connell LD, Elsworth D. Influence of the effective stress coefficient and sorption-induced strain on the evolution of coal permeability: Model development and analysis. Int J Greenh Gas Contr 2012;8:101–10.
[47] Niu QH, Cao LW, Sang SX, Zhou XZ, Wang ZZ. Anisotropic adsorption swelling and permeability characteristics with injecting CO_2 in coal. Energy Fuels 2018;32(2):1979–91.
[48] Evans JP, Forster CB, Goddard JV. Permeability of fault-related rocks, and implications for hydraulic structure of fault zones. J Struct Geol 1997;19 (11):1393–404.
[49] Jasinge D, Ranjith PG, Choi SK. Effects of effective stress changes on permeability of Latrobe valley brown coal. Fuel 2011;90(3):1292–300.
[50] Perera MSA, Ranjith PG, Viete DR. Effects of gaseous and super-critical carbon dioxide saturation on the mechanical properties of bituminous coal from the Southern Sydney Basin. Appl Energy 2013;110:73–81.
[51] Pan ZJ, Connell LD, Camilleri M. Laboratory characterisation of coal reservoir permeability for primary and enhanced coalbed methane recovery. Int J Coal Geol 2010;82(3–4):252–61.
[52] Zhang XG, Ranjith PG, Ranathunga AS, Li DY. Variation of mechanical properties of bituminous coal under CO_2 and H_2O saturation. J Nat Gas Sci Eng 2019;61:158–68.